

An asynchronous time-stepping (ATS) integrator for atmospheric applications: Aerosol dynamics

K. Max Zhang^{a,*}, Anthony S. Wexler^{a,b,c}

^a*Department of Mechanical and Aeronautical Engineering, University of California, Davis, CA 95616, USA*

^b*Department of Civil and Environmental Engineering, University of California, Davis, CA 95616, USA*

^c*Department of Land, Air, and Water Resources, University of California, Davis, CA 95616, USA*

Received 29 September 2005; received in revised form 7 February 2006; accepted 24 March 2006

Abstract

Mixed time integration methods, also known as multiple time-step methods (MTS), have been proposed and implemented successfully to reduce the stiffness of problems in molecular dynamics and solid mechanics, where different time scales are used to integrate different motions or meshes. We apply the similar concept and develop an asynchronous time-stepping (ATS) integrator for atmospheric application. This paper first presents ATS as a generalized ordinary differential equation solver and describes its key components including: (1) global and local time management; (2) dynamic time-scale ordering; and (3) integration and iteration methods. Then we apply ATS to solve stiff problems in aerosol dynamics, where we further introduce several techniques such as grouping particulate species by particle sections to speed up computations. The comparisons between ATS and standard ODE solvers including LSODE, LSODES and VODE in aerosol dynamics simulation are presented, which show that ATS is robust and able to achieve a significant digit average (SDA) value of 2.0 to 3.0 while its speed is around 10 to 100 times faster than LSODE with equivalent accuracy. ATS has been implemented in CMAQ-UCD, a sectional, dynamic aerosol model built on USEPA's CMAQ platform.

© 2006 Elsevier Ltd. All rights reserved.

Keywords: Stiff problem; Ordinary differential equations (ODE); MTS; Aerosol dynamics; CMAQ-UCD

1. Introduction

Numerical simulations of physical systems often contain high frequency and low frequency degrees of freedom. In molecular dynamics, for example, the bond vibrations usually occur on a time scale which is short compared to that of the translations and rotations (Tuckerman et al., 1990). In path integral simulations of electron salvation, the vibrational

force constants arising from the kinetic energy operator increase linearly with the size of the chain (Wu and Smolinski, 2000). Hence, the vibrations of the chain are often fast compared with any other motion in the system. Standard integrators require the choice of time step sufficiently small to guarantee stable solution of the highest frequency motion with the consequence that simulations require a very large number of CPU cycles (Tuckerman et al., 1990). In solid mechanics, the mesh of a finite element model is not uniform in that material properties and element sizes can vary

*Corresponding author. Fax: 530 752 4158.

E-mail address: maxzhang@ucdavis.edu (K.M. Zhang).

widely throughout the mesh. For explicit time integration the stable time step is based on the maximum frequency of the mesh and if there is a small region of elements with high frequencies it will set a small critical time step for the entire problem. Also, if a problem has localized loads that vary rapidly, a small time step is necessary to accurately capture the behavior of the load even though far from the load a larger time step may give adequate accuracy (Wu and Smolinski, 2000).

Similar problems also arise in atmospheric applications. The chemical process describing the fate of atmospheric pollutants is mathematically represented through a set of coupled, nonlinear ordinary differential equations (ODEs). A primary source of difficulty in the numerical solution of these equations arises from the fact that the gas chemistry or aerosol dynamics in atmospheric systems involves reactions or gas/particle mass transfer whose characteristic time scales vary orders of magnitude, resulting in highly “stiff” and large systems of equations. For instance, the stiffness ratio for ODEs arising from typical tropospheric photochemistry system is usually of the order of 10^{10} . The system to simulate aerosol dynamics can also be very stiff, partly because atmospheric particle size range spans diameters from a few nanometers to tens of microns. Since the mass transfer rate between gaseous and particulate phases is strongly dependent on particle size, the mass transfer rates for the smallest and the largest particles may differ by several orders of magnitude. The causes of stiffness in simulating aerosol dynamics will be elaborated in Section 3. Further, the spatial dependencies typical of three-dimensional (3D) air quality models require solution of these equations at each computational node of the modeled domain, resulting in an extremely computationally intensive problem. Although computational power has increased tremendously in recent years and significant advances have been made in the numerical solution of stiff ODEs for atmospheric applications (Young and Boris, 1977; Hesstvedt et al., 1978; Hertel et al., 1993; Sun and Wexler, 1998; Capaldo et al., 2000), the emerging long-term studies, such as annual air quality and global climate change simulations, and regulatory studies such as SIPs, which simulate the same episodes numerous times under various control scenarios, pose greater computational demands. So the search for faster and more accurate solution methodologies is of considerable interest

to atmospheric modelers, because a major portion of the computational efforts in comprehensive atmospheric chemistry/transport models is devoted to solving these kinetic equations (Mathur et al., 1998).

Mixed time integration methods, also known as multiple time-step methods (MTS), have been proposed and implemented successfully to reduce the stiffness of problems in molecular dynamics (Streett et al., 1978; Tuckerman et al., 1990) and solid mechanics (Belytschko and Mullen, 1976; Neal and Belytschko, 1989; Belytschko and Lu, 1993; Smolinski and Wu, 1998; Wu and Smolinski, 2000), where different time scales are used to integrate different motions or meshes. In this paper, we apply a similar concept and develop an asynchronous time-stepping (ATS) integrator for atmospheric applications, i.e., gas chemistry and aerosol dynamics. The current paper describes the ATS algorithm and compares its predictions to those from established ODE solvers for aerosol dynamics calculations. This paper is organized as follows: we first present ATS as a generalized ODE solver; the causes of stiffness, customized ATS formulations and comparisons to accurate ODE solvers in aerosol dynamics are discussed, respectively. The two following papers will discuss its implementation in simulating aerosol dynamics (Zhang and Wexler, 2006; Nolte et al., 2006) in 3-D air quality models.

2. ATS as a generalized ODE solver

2.1. ATS' computational advantages

Stiffness occurs because there are a wide range of time scales in the solution. A set of ODEs of the form

$$\frac{dc_i}{dt} = f_i(c_j, t), i, j = 1, 2, \dots, n \quad (1)$$

is stiff if (1) the eigenvalues of the Jacobian matrix of the system are negative, i.e. $\text{Re}(\lambda_i) < 0$, $i = 1, 2, 3, \dots, n$; and (2) the ratio of the maximum to the minimum eigenvalues, $\max|\text{Re}(\lambda_i)|/\min|\text{Re}(\lambda_i)| \gg 1$ (Lambert, 1980). Instead of solving this set of equations simultaneously, multiple time-step (MTS) methods use a small time step δt to advance the fast equations n steps holding the slow variables fixed; the slow degrees of freedom are then updated using a time step $n\delta t$ (Swindoll and Haile, 1984; Telemann and Jönsson, 1986). The main computational advantages of MTS/ATS over other synchronous

time-stepping methods are: (1) the number of integrations over slow variables is greatly reduced; and (2) the inversion of Jacobin matrix can be avoided. These advantages become more evident as the system becomes larger and stiffer. However, simply holding slow variables constant will inevitably lead to loss of accuracy. We take several measures to enhance the accuracy of ATS while keeping its competitive speed advantage.

2.2. Time Management and Dynamic Ordering in ATS

ATS consists of two timing systems, i.e., global time and local time. While the former applies to every variable universally, the latter is variable-dependent. The current global time is t_{curr} . The characteristic time scale for a variable in an general ODE form of $dc_i/dt = f_i$ at t_{curr} is $\tau_i = c_i/f_i$, $i = 1, 2, \dots, n$. The integration time scale is $\epsilon\tau_i$, where ϵ is a small number used to maintain stability and also a prescribed tolerance for error control. We sort the order of variables by their integration time scale at t_{curr} . The target global time, t_{new} , is set to be $t_{curr} + \epsilon\tau_{i,max}$, where $\tau_{i,max}$ is the largest integration time scale among all variables. We call the integration from t_{curr} to t_{new} a “pass” (Fig. 1). At the beginning of each pass, the local times, $t_{i,local}$, for all variables are synchronized at t_{curr} . Then, the local time of each variable is updated by increments of its

own integration time scale. Therefore, the local times within a pass are asynchronous.

The integration starts from the variable with the smallest time scale, i.e., the “fastest” variable. Next, the timing is checked before integration of the remaining variables in the order of increasing integration time scales. A variable, c_i , will not be integrated until the local time of the variable with next smaller time scale, c_j , reaches or passes the mid point between c_i ’s local time and target local time, $t_{i,local} + \epsilon\tau_i$ (Fig. 2). A “scan” is the process of checking which equations should be integrated (Fig. 1). Although all variables are checked in a scan, not all variables are actually integrated. In case of very stiff problems, where the characteristic time scales may differ by several orders of magnitudes, fast variables will be integrated many times before slow variables advance. When the local time of every variable reaches the target global time, t_{new} , a pass is completed and a new pass initiates. This cycle goes on until the global time reaches the intended termination time.

In many applications, variables are strongly coupled. Since the order may change within a pass as the time scales change, the order is sorted after every scan, thus ensuring that faster variables are always integrated before slower ones. When integrating slower variables, the current values of faster ones are used. When integrating faster variables, slower variables have been held constant in previous applications. To increase accuracy, we implement a

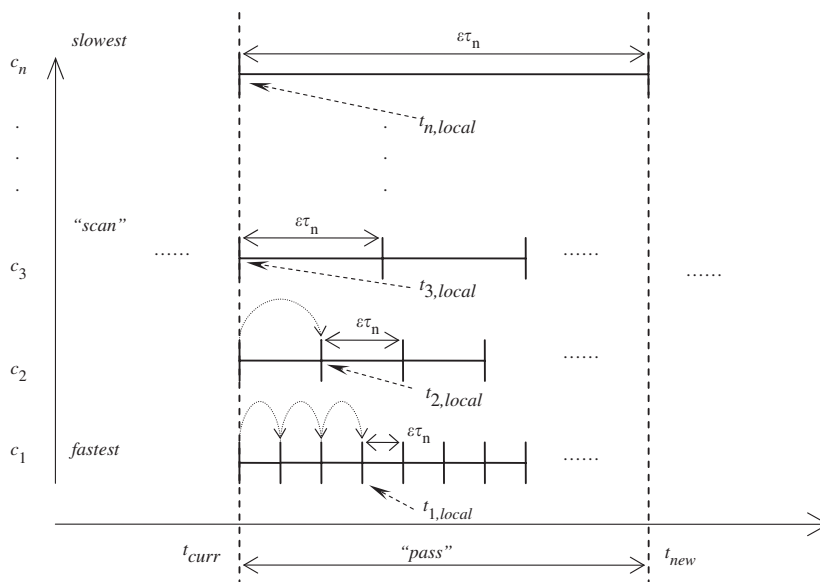


Fig. 1. A sketch of ATS time management scheme where local times are asynchronous.

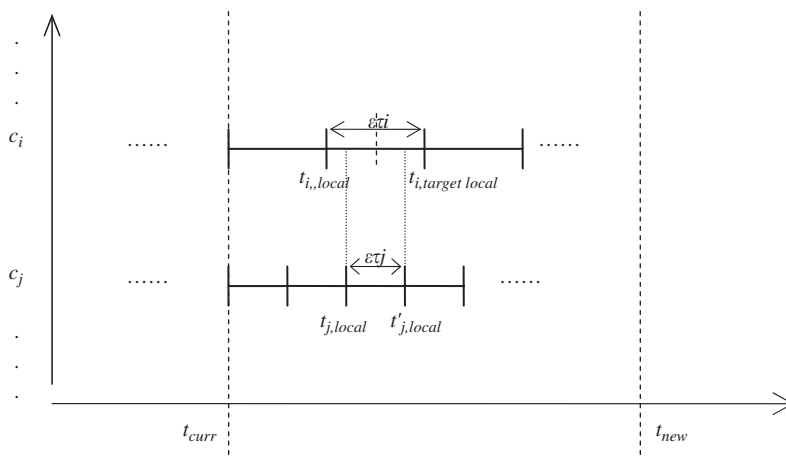


Fig. 2. Variable c_i advances only when c_j , the variable with next smaller time scale, reaches or passes the halfway-point between c_i 's local time and target local time. An interpolated/extrapolated value of c_i is used when c_j is being integrated.

linear interpolation/extrapolation predictor and corrector scheme to acquire the values of slow variables corresponding to the local time of fast variables. Since the time scales of faster variables are usually much shorter than those of slower ones, linear interpolation/extrapolation is sufficient approximation in most of cases. However, linear approximation would lead to serious errors when the time scales of some slower variables are only slightly larger than that of fast ones. In such cases, we employ an exponential interpolation/extrapolation to replace linear approximation (Fig. 2).

2.3. Integration and Iteration methods in ATS

We adopt the backward differentiation formulae (Gear, 1971), an implicit integration scheme, and a modified Newton iteration scheme in ATS. The general form of the backward differentiation formulae (BDF) is

$$c_{n+k} = h\beta_k f_{n+k} - \sum_{j=0}^{k-1} \alpha_j c_{n+j}, \quad (2)$$

where α and β are coefficients with $\alpha \neq 0$ and $\beta \neq k$, and the order is equal to the step number, k . For orders one to six these methods are stiffly stable. The first order method is the backward Euler method.

Since Eq. (2) is implicit, it must be solved iteratively by using Newton's method of the form

$$c^{(m+1)} = c^{(m)} - F(c^{(m)}) \cdot J^{-1}(c^{(m)}), m = 0, 1, \dots, \quad (3)$$

where m is the iteration index; $F(c) = 0$; J is the Jacobian of the system (Oran et al., 1987). Rather

than inverting the Jacobian, we only iterate the equation for c_i , so

$$c_i^{(m+1)} = c_i^{(m)} - \frac{f(c_i^{(m)})}{f'(c_i^{(m)})}. \quad (4)$$

3. Application of ATS in Aerosol Dynamics

3.1. Stiffness in Aerosol Dynamics

The rate equations for gas photochemistry problems can either take the general form of Eq. (1) or be cast in the following ‘‘source’’ and ‘‘sink’’ manner:

$$\frac{dc_i}{dt} = Q_i(\text{source}) + L_i \cdot c_i(\text{sink}), \quad (5)$$

where Q_i is positive-definite production rate and L_i is the negative-definite loss rate. A number of approaches have been proposed over the years to efficiently solve this stiff problem (Young and Boris, 1977; Hesstvedt et al., 1978; Hertel et al., 1993).

Compared to gas chemistry, efforts to reduce stiffness in aerosol dynamics were investigated much more recently. A system representing aerosol dynamics consists of both gaseous and particulate species. Gas/particle mass transfer is the major portion of aerosol dynamics, whose governing equation for an internally mixed particle population with its size distribution described by N discrete size sections is (Wexler et al., 1994)

$$\frac{\partial p_i^j}{\partial t} = H_i^j p_i^j(\text{growth}) - \frac{1}{3} \frac{\partial H^j p_i^j}{\partial \mu}(\text{shift}), \quad (6)$$

and for gaseous species is

$$\frac{\partial c_i}{\partial t} = -r_{\text{MW}} \sum_{j=1}^N H_i^j p^j. \quad (7)$$

Mass conservation of species i requires

$$r_{\text{MW}} \sum_{j=1}^N p_i^j + c_i = \text{const.} \quad (8)$$

In Eqs. (6)–(8), p_i^j is the mass distribution of the particulate species i in the j th section; μ is the log of the particle diameter; H_i^j is the condensation/evaporation rate of the particulate species i in the j th section, with units of s^{-1} ; $H^j = \sum_{i=1}^s H_i^j$ and $p^j = \sum_{i=1}^s p_i^j$, and s is the number of particle compounds simulated; c_i is the concentration of the gaseous species i ; r_{MW} is a unitless factor accounting for differences in molecular weight between the same compounds (such as NH_4 and NH_3) in the gaseous and particulate forms. Numerically, the difference between aerosol dynamics and gas chemistry is that the evaluation of H terms on the right hand side of Eq. (6) requires computationally intensive, structurally complex aerosol thermodynamics calculations, whereas the production and loss rate terms in Eq. (5) only need simple mathematical manipulations in gas chemistry simulations.

Thus each gaseous species is represented by an ODE in the form of Eq. (7). Each particulate species in every section is represented by Eq. (6), consisting both an ODE and a PDE as its first and second terms on the right-hand side, respectively. The two terms are usually simulated separately and ATS is only used to solve the ODE part, i.e., the “growth” term. Aerosol dynamics systems usually contain organic and inorganic species. In this paper, we confine our attentions to the inorganics. For typical urban inorganic aerosol compositions which contain NH_3 , HCl , HNO_3 and H_2SO_4 in the gaseous phase and H^+ , NH_4^+ , Na^+ , Cl^- , NO_3^- , SO_4^{2-} in the particulate phase, the total number of equations in this system is $4+6N$, where N is the number of discrete size sections as mentioned earlier.

As defined in the beginning of Section 2.1, the characteristic time scale for a particulate species is

$$\tau_{i,p}^j = \frac{p_i^j}{H_i^j p^j}, \quad (9)$$

and for a gaseous species is

$$\tau_{i,g}^j = \frac{c_i}{r_{\text{MW}} \sum_{j=1}^N H_i^j p^j}. \quad (10)$$

Note that H_i^j , which is the characteristic time over which the particle size j changes due to condensation of compound i , can be expressed as

$$\begin{aligned} H_i^j &= \frac{1}{m^j} \frac{dm_i^j}{dt} = \frac{12D_i}{(D_p^j)^2 \rho_p (1+\gamma)} (c_i - c_{i,\text{surf}}^j) \\ &= \frac{1}{A^j F} (c_i - c_{i,\text{surf}}^j). \end{aligned} \quad (11)$$

By combining (9) and (11), the expression for the characteristic time scale for a particulate species can be simplified to

$$\tau_{i,p}^j = \frac{m_i^j}{dm_i^j/dt}. \quad (12)$$

In Eq (11), m_i^j is the mass of species i in an individual particle of total mass m^j ; D_i is the gas-phase diffusion coefficient of species i ; ρ_p is the particle density; c_i and $c_{i,\text{surf}}^j$ are its mass concentrations in the gas phase and over the particle surface, respectively; the factor γ accounts for the non-continuum effects and the imperfect accommodation of the condensate on the particle surface, the latter of which is described by the accommodation coefficient, α_i ; $F = \rho_p/(12D_i)$, which is size-independent (when ρ_p is regarded as constant), and $A^j = (D_p^j)^2 (1+\gamma)$. For most purposes, a sufficient approximation is $\gamma = 8D_i/\alpha_i c_i D_p^j \approx 8\lambda/\alpha_i D_p^j$ (Wexler and Seinfeld, 1990), where c_i is the mean thermal molecular velocity of species i in air, and λ is the air mean free path (around $0.065 \mu\text{m}$ at 298 K).

Two major factors contribute to stiffness in aerosol dynamics: composition and particle size. Composition-wise, the concentration of some species may change rapidly with the condensation or evaporation of other species. A typical example is hydrogen ion in near-neutrality conditions. For hydrogen ion its characteristic time scale, in the form of Eq. (12), can be expressed as $\tau_{\text{H}} = |m_{\text{H}}/(dm_{\text{H}}/dt)|$, and for other species, $\tau_i = |m_i/(dm_i/dt)|$, where i is either NH_3 , HNO_3 or HCl . Note that the superscription j is neglected here since we are dealing with particulate components in the same size section. The quantities dm_{H}/dt and dm_i/dt are of the same order because dm_i/dt for the acid/base compounds results in dm_{H}/dt . Therefore a very

small m_H leads to a value of τ_H much smaller than that of the others τ_i 's. Mathematically, these different time scales lead to a system of stiff differential equations, in which a very small time step, on the order of τ_H , must be chosen to integrate the equations numerically, even though the actual rate of concentration changes, τ_i , would allow us to use much larger time steps (Sun and Wexler, 1998). Sun and Wexler (1998) assume that as long as the near acid neutral condition is maintained, the aerosol hydrogen ion concentration will stay at a constant level. This effectively puts a constraint on the way in which ammonia, nitric acid, hydrochloric acid and sulfuric acid condense and evaporate, analogous to the pseudo-steady state approximation frequently adopted in gas phase chemistry. The resultant gas–particle transfer scheme, H^+ -independent in formulation, is called “coupled transport” (Sun and Wexler, 1998).

As touched upon in the *Introduction*, the broad size range of atmospheric particles also leads to stiffness. Using Eq. (9), let us compare the characteristic time scales for two different size bins (denoted by superscripts j and k):

$$\frac{\tau_j^j}{\tau_i^k} = \frac{p_i^j/H_i^j p^j}{p_i^k/H_i^k p^k} = \left(\frac{H_i^k}{H_i^j}\right) \left(\frac{p^k}{p^j}\right) \left(\frac{p_i^j}{p_i^k}\right). \quad (13)$$

Suppose that all size particle sections have similar concentrations and compositions, which leads to an approximation of Eq. (13) as

$$\frac{\tau_j^j}{\tau_i^k} \approx \frac{H_i^k}{H_i^j} \approx \frac{A^j}{A^k}. \quad (14)$$

Most of the parameters in the expression of A have been noted after Eq. (11). In a common 8-size section formulation the mean diameter of the largest section is $7.07 \mu\text{m}$ while the diameter of the smallest section is $0.055 \mu\text{m}$. In addition, we assume the accommodation coefficient α to be a constant value ($= 0.6$). Applying these values, the factor A is around $0.05 \mu\text{m}^2$ for the smallest size bin and $56 \mu\text{m}^2$ for the largest size bin. Thus the characteristic time scales have three orders of magnitude difference. The mathematical description of such systems results in a set of extremely stiff differential equations.

One solution to stiffness caused by large range of particle sizes has been proposed by Capaldo et al. (2000), who suggested a hybrid method that combines some of the speed of the equilibrium methods with the accuracy of the dynamic methods.

The hybrid method employs an equilibrium approach to determine the composition of the small particles and uses the multicomponent aerosol dynamic model (MADM) of Pilinis et al. (2000) to calculate the mass transfer to larger particles. Here we use ATS to avoid an equilibrium assumption.

3.2. ATS for Aerosol Dynamics

Next, we describe how ATS is constructed to reduce the stiffness in aerosol dynamics. As discussed earlier, in gas phase photochemistry, the right hand side of the ODEs is computationally inexpensive to evaluate. Such is not the case for aerosol dynamics where computationally intensive thermodynamics determines the surface equilibrium concentrations of the volatile species (i.e., the $c_{i,\text{surf}}^j$ term in Eq. (11)). Therefore, it is not numerically feasible to solve the system of aerosol dynamics as a set of generalized ODE's. On the other hand, the characteristics of aerosol dynamics enable us to employ some strategies that speed up the integrating process.

3.2.1. ODE grouping by particle sections

Eqs. (8) and (11) show that gas/particle transport, also known as condensation/Evaporation, of a species is governed by its gas phase concentration, c_i , and equilibrium concentration over the particle surface, $c_{i,\text{surf}}$. In the sectional approach, the same species in different size sections may have different equilibrium surface concentrations. The equilibrium surface concentration of a species is determined by its interaction with other electrolytes existing in that size section as well as meteorological conditions such as ambient temperature and relative humidity. Particulate components in a size bin do not directly interact with those in other bins but rather through the gas phase, in other words, molar conservation of the total concentration of each species in each integration step as formulated in Eq. (8). Take ammonia as an example: the equilibrium vapor pressure of NH_4^+ in size section A is independent of the NH_4^+ concentration in size section B . However, molar conservation of ammonia requires

$$r_{\text{MW}} \sum_{j=1}^N p_{\text{NH}_4}^j + c_{\text{NH}_3} = \text{const.},$$

where N is the total number of size sections.

Summarizing, in aerosol dynamics we have strong coupling among particulate components in the same

size section, weak coupling through the gas phase among the same component in different sections and even weaker coupling between different components in different sections. In addition, it is common to assume thermodynamic equilibrium within the section so that one thermodynamic calculation predicts the equilibrium concentration of all volatile species. Thus in ATS, we group the particulate species by size section. The time scale of each section is dictated by the species with the smallest time scale in that section.

3.2.2. Near-equilibrium conditions and stability check

Splitting the “shift” term in Eq. (6), we can reorganize its right-hand side into “source” and “sink” format similar to that for gas chemistry, i.e., Eq. (5):

$$\frac{\partial p_i^j}{\partial t} = H_i^j \sum_{k \neq j} p^k + H_i^j p_i^j.$$

Different from that of gas chemistry species, the eigenvalue here is positive as condensation occurs. Although this expression may appear to be mathematically unstable, it is in fact stable since H_i^j always approaches zero as gas and particle compositions evolve towards equilibrium. Also, in aerosol dynamics, concentrations in either phase are constrained by mass conservation, as described by Eq. (8), at each integration step. So the concentrations are bounded even when numerical stability deteriorates in contrast to gas chemistry simulations, where mass conservation is implied rather than forced in the expressions of ODEs.

Although aerosol dynamics is driven towards thermodynamic equilibrium between gas and particulate phases, this equilibrium is perturbed by several factors, such as temperature, relative humidity and emissions (Zhang and Wexler, 2004). In typical urban environments, the temperature and relative humidity change following a diurnal pattern. In other words, under urban background conditions aerosol thermodynamic states are typically near equilibrium because the perturbation timescale is around one day whereas the characteristic aerosol timescales are typically shorter than one hour.

As discussed earlier, we adopt an implicit integration scheme to solve the gas chemistry. Nevertheless, the implicit integration exerts some computational challenges for aerosol dynamics

simulation, since the full thermodynamic calculation has to be implemented for every iteration step.

Considering all the factors presented above, we employ an explicit Euler integration method in ATS. Stability is primarily controlled by choosing an appropriate value for ε , the prescribed tolerance. We also adopt a predictor and corrector scheme to further maintain stability. Instability will lead to unrealistic conditions, which are most likely to happen during acidity transitions. In the presence of volatile acids and bases in the gas and particle phase, the condensation or evaporation of those compounds will tend to drive the aerosol phase toward acid neutrality. This neutrality will persist as long as volatile materials are not depleted from either phase. So under such circumstances the only possible transitions are from basic to neutral to acidic or from acidic to neutral to basic. The aerosol model must guarantee the transitions accurately followed. However, unrealistic jumps in pH could occur if the time step is inappropriately chosen since the pH time scale is so short. For example, suppose we have acidic particles with ammonia in the gas phase. The thermodynamics favors condensation of ammonia to neutralize aerosols. Instability could predict an ammonia overshoot leading to an unrealistically large amount of ammonia condensing so that the aerosols become basic. In ATS, pH transition past neutral is checked after each integration. If unrealistic transition takes place, the time step is reduced until the correct transition order occurs.

3.3. Comparison with Standard ODE Solvers

In most previous comparative studies, methods of interest have been tested against Gear’s (Gear, 1971) method, which employs a variable-order backward differentiation, constrained by strict tolerance limits to provide extremely accurate solutions for a particular test problem. The LSODE (Livermore solver for ordinary differential equations) and LOSDES (Livermore solver for ordinary differential equations with general sparse Jacobian matrix.) are the two most widely used Gear variants (Hindmarsh, 1983; Eisenstat et al., 1977, 1982). In addition, a relatively recent development, VODE (Variable-coefficient ordinary differential equation solver with fixed-leading-coefficient implementation), which adopts multistep methods with full variable step sizes and coefficients, is also chosen for

comparison purposes (Hindmarsh, 1983; Brown et al., 1989).

We test the ATS solver using the inorganic aerosol system described in Table 1. This system contains four gas phase species and seven particulate species in nine size sections. Since we model water as an equilibrium species, there are seven actively integrated particulate species. Thus the total number of ODEs is $4+6=58$. To compare the performance of ATS in relation to the other solvers, we apply the same thermodynamic module for these integration schemes. Considering the strong geographical dependence of aerosol compositions, we choose compositions in Tampa, FL; Bakersfield, CA; Los Angeles, CA and Riverside, CA for testing. The initial gas phase and size-resolved particulate concentrations used in the test cases were acquired by reconstructing the measurement data collected in Tampa (Campbell et al., 2002), Bakersfield (Herner et al., 2005), Los Angeles and Riverside (Allen et al., 2000). They represent the typical compositions in Tampa's summer season, Bakersfield's winter season and Los Angeles/Riverside's summer season.

For each location, we tested both the condensation and evaporation scenarios. We found that gas-phase and particulate-phase concentrations measured in Tampa were very close to equilibrium, so we artificially perturbed the gas phase concentrations to simulate condensation and evaporation cases. First we increase the $\text{HNO}_3(\text{g})$ and $\text{NH}_3(\text{g})$ concentration to simulate a condensation scenario. Then the predicted particulate concentrations after a 12 min simulation and the measured gas phase concentrations were used to simulate an evaporation scenario. Bakersfield data were clearly a condensation case, and so similarly, we decrease the $\text{HNO}_3(\text{g})$ and $\text{NH}_3(\text{g})$ concentrations combined with 12 min' simulated particulate concentrations to simulate an evaporation scenario. Similarly, we create the condensation and evaporation cases for Los Angeles and Riverside. We pick 12 min as a standard integrating time chunk since it

is a typical time step in 3-D Eulerian air quality models.

We set the tolerance of LSODE to be rather strict: 10^{-6} RTOL/ 10^{-10} ATOL for Tampa cases, 10^{-5} RTOL/ 10^{-8} ATOL for Bakersfield cases, 10^{-9} RTOL/ 10^{-6} ATOL for Los Angeles and 10^{-7} RTOL/ 10^{-8} ATOL for Riverside. With such strict tolerances, the results from LSODE are considered to be "exact". For each individual case, we also test ATS with $\varepsilon = 0.1$ and 0.01, respectively. We did not simulate smaller ε values since it would become computationally unrealistic when implemented in 3-D air quality models.

The metrics we adopt for the comparisons are normalized error, root-mean-square error (RMSE) and number of significant digits for the average (SDA) of RMSE (Verwer et al., 1996). The normalized errors are listed for each species in each section for one test case. The RMSE value, based on Eq. (15), represents the sum of all species in all sections in each individual test case.

$$\text{RMSE}_K = \sqrt{\frac{1}{M} \sum_{m=1}^M \left(\frac{c_k^m - \hat{c}_k^m}{\hat{c}_k^m} \right)^2}, \quad (15)$$

SDA, defined as

$$\text{SDA} = -\log_{10} \left(\frac{1}{n} \sum_{k=1}^n \text{RMSE}_k \right), \quad (16)$$

is calculated on RMSE values from all eight cases.

The normalized errors resulting from each case are tabulated in Tables 2–9. Among all the species, usually sulfate has the smallest error; its vapor pressure is essentially zero so that it is uncoupled from other species. Considering particle size, errors are low for the larger size sections because they are not very dynamic, the converse being true for the smaller particle sizes.

The RMSE and SDA values along with CPU times are summarized in Table 10. These benchmark parameters are obviously case-dependent. The eight testing cases generally cover typical scenarios

Table 1
Model parameters

Species	$\text{NH}_3(\text{g})$, $\text{HNO}_3(\text{g})$, $\text{HCl}(\text{g})$, $\text{H}_2\text{SO}_4(\text{g})$, H^+ , NH_4^+ , Na^+ , SO_4^{2-} , NO_3^- , Cl^- , H_2O (total 11 species)
Size cuts (μm)	0.039-0.078, 0.078-0.156, 0.156-0.312, 0.312-0.625, 0.625-1.25, 1.25-2.5, 2.5-5.0, 5.0-10.0, 10.0-20.0 (total 9 sections)
Integration time (min)	12

Table 2

Normalized errors for Tampa condensation case. ATS: $\varepsilon = 0.1$ (left column) and 0.01(right column); LSOE: RTOL = 10^{-6} , ATOL = 10^{-10}

Size bin	NH ₄ ⁺		SO ₄ ²⁻		NO ₃ ⁻		Cl ⁻		H ₂ O	
1	-0.3836%	-0.0799%	-0.3874%	-0.0830%	-0.3452%	-0.0797%	2.9600%	-0.1891%	-0.3752%	-0.0819%
2	0.0648%	-0.0054%	0.0582%	-0.0042%	-0.0718%	-0.0045%	0.2582%	-0.1242%	0.0481%	-0.0058%
3	0.0513%	0.0128%	0.0494%	0.0099%	0.0043%	0.0192%	0.1573%	-0.0740%	0.0554%	0.0139%
4	0.0722%	0.0093%	0.0711%	0.0142%	-0.0963%	0.0153%	-0.0403%	-0.0806%	0.0598%	0.0100%
5	0.0121%	0.0060%	0.0106%	0.0032%	-0.0427%	0.0244%	0.0563%	-0.0844%	0.0072%	0.0072%
6	-0.0213%	0.0071%	0.0071%	-0.0071%	-0.0140%	-0.0195%	-0.0369%	0.0821%	-0.0081%	0.0081%
7	-0.0048%	0.0095%	0.0067%	0.0034%	0.0085%	-0.0053%	-0.0161%	0.0107%	-0.0072%	0.0024%
8	0.0000%	0.0053%	0.0045%	0.0000%	0.0000%	-0.0052%	-0.0014%	0.0042%	0.0000%	-0.4738%
9	0.0000%	0.0000%	0.0000%	0.0000%	0.0000%	-0.0019%	0.0000%	0.0000%	-0.0014%	0.0000%
Gas	NH ₃ (g)		H ₂ SO ₄ (g)		HNO ₃ (g)		HCl(g)			
	-0.0048%	0.0002%	-1.1808%	-0.1352%	0.0051%	0.0059%	-1.1808%	-0.1352%		

Table 3

Normalized errors for Tampa condensation case. ATS: $\varepsilon = 0.1$ (left column) and 0.01(right column); LSOE: RTOL = 10^{-6} , ATOL = 10^{-10}

Size bin	NH ₄ ⁺		SO ₄ ²⁻		NO ₃ ⁻		Cl ⁻		H ₂ O	
1	-0.0082%	0.0082%	0.0000%	0.0030%	-2.3143%	-0.0329%	9.8070%	-0.1305%	-0.0025%	0.0000%
2	0.0000%	0.0000%	0.0000%	0.0000%	-0.1376%	0.0512%	-0.3108%	0.2284%	0.0017%	0.0017%
3	-0.0080%	0.0000%	0.0000%	0.0000%	0.5273%	-0.0213%	2.0240%	-0.1301%	0.0082%	0.0000%
4	0.0057%	0.0000%	0.0000%	0.0000%	-0.6714%	-0.0198%	-2.1997%	-0.1072%	-0.0119%	-0.0059%
5	-0.0032%	0.0000%	0.0000%	0.0000%	0.1014%	-0.0235%	0.7383%	-0.1170%	0.0000%	0.0000%
6	0.0399%	0.1340%	0.0000%	0.0000%	0.0258%	0.0452%	0.0121%	0.2064%	0.0097%	0.0389%
7	0.0058%	0.0289%	0.0000%	0.0000%	-0.0022%	0.0011%	0.0061%	0.0182%	0.0000%	0.0077%
8	-0.0118%	0.0059%	0.0000%	0.0000%	-0.0035%	0.0000%	-0.0044%	0.0015%	-0.0025%	0.0025%
9	0.0000%	0.0000%	0.0028%	0.0028%	-0.0019%	0.0000%	0.0000%	0.0000%	-0.0014%	0.0000%
Gas	NH ₃ (g)		H ₂ SO ₄ (g)		HNO ₃ (g)		HCl(g)			
	0.0011%	-0.0114%	-5.6760%	-0.7667%	0.0015%	-0.0130%	-0.0043%	-0.1268%		

Table 4

Normalized errors for Bakersfield condensation case. ATS: $\varepsilon = 0.1$ (left column) and 0.01(right column); LSOE: RTOL = 10^{-5} , ATOL = 10^{-8} . Section 9 ($> 10 \mu\text{m}$) data is not available

Size bin	NH ₄ ⁺		SO ₄ ²⁻		NO ₃ ⁻		Cl ⁻		H ₂ O	
1	-3.7955%	-0.3027%	-2.6326%	-0.0533%	-3.8862%	-0.3915%	N/A	N/A	-3.9357%	-0.4446%
2	-0.8906%	-0.0388%	-0.0241%	0.0080%	-0.9835%	-0.0393%	N/A	N/A	-0.8931%	-0.0363%
3	-0.0957%	-0.0186%	0.0000%	0.0045%	-0.0919%	-0.0200%	-0.0235%	-0.0078%	-0.0730%	-0.0162%
4	0.0112%	0.0000%	0.0000%	0.0000%	0.0084%	0.0000%	-0.0035%	-0.0052%	0.0086%	0.0000%
5	0.0148%	0.0033%	0.0046%	0.0046%	0.0157%	0.0000%	-0.0014%	-0.0028%	0.0117%	0.0029%
6	0.0098%	0.0000%	0.0035%	0.0035%	0.0078%	0.0000%	-0.0035%	-0.0035%	0.0046%	0.0000%
7	-0.4893%	-0.4934%	0.0100%	0.0100%	-0.0489%	-0.0783%	0.0000%	0.0000%	-0.1783%	-0.1783%
8	-0.1103%	-0.1103%	0.0000%	0.0000%	-0.0199%	-0.0199%	0.0000%	0.0000%	-0.0192%	-0.0192%
9	N/A	N/A	N/A	N/A	N/A	N/A	N/A	N/A	N/A	N/A
Gas	NH ₃ (g)		H ₂ SO ₄ (g)		HNO ₃ (g)		HCl(g)			
	0.0001%	0.0007%	N/A	N/A	-0.0274%	0.0082%	0.0076%	-0.0010%		

Table 5

Normalized errors for Bakersfield evaporation case. ATS: $\varepsilon = 0.1$ (left) and 0.01 (right); LSODE: RTOL = 10^{-5} , ATOL = 10^{-8} . Section 9 ($> 10 \mu\text{m}$) data is not available

Size bin	NH ₄ ⁺		SO ₄ ²⁻		NO ₃ ⁻		Cl ⁻		H ₂ O	
1	3.1794%	-0.1918%	-2.6326%	0.0761%	4.2495%	-0.1999%	-5.2385%	-0.2028%	2.6746%	-0.1900%
2	-0.5414%	-0.0422%	-0.0241%	0.0000%	-0.7020%	-0.0541%	-0.1567%	-0.0265%	-0.5264%	-0.0361%
3	0.0171%	0.0014%	0.0000%	0.0045%	0.0196%	0.0039%	-0.0386%	0.0000%	0.0123%	0.0020%
4	0.0114%	0.0000%	0.0000%	0.0000%	0.0171%	0.0000%	-0.0316%	0.0000%	0.0044%	0.0000%
5	-0.0034%	0.0000%	0.0046%	-0.0046%	-0.0054%	0.0000%	0.0214%	0.0000%	0.0000%	0.0000%
6	0.0000%	0.0000%	0.0035%	0.0000%	0.0000%	-0.0025%	0.0037%	0.0037%	-0.0011%	-0.0011%
7	0.0000%	0.0000%	0.0100%	0.0000%	0.0089%	0.0000%	0.0000%	0.0000%	0.0000%	0.0000%
8	0.0000%	0.0000%	0.0000%	0.0000%	0.0000%	0.0000%	0.0000%	0.0000%	0.0010%	0.0000%
9	N/A	N/A	N/A	N/A	N/A	N/A	N/A	N/A	N/A	N/A
Gas	NH ₃ (g)		H ₂ SO ₄ (g)		HNO ₃ (g)		HCl(g)			
	-0.0058%	-0.0004%	N/A	N/A	-0.0391%	0.0014%	0.1544%	-0.0032%		

Table 6

Normalized errors for Los Angeles condensation case. ATS: $\varepsilon = 0.1$ (left) and 0.01 (right); LSODE: RTOL = 10^{-9} , ATOL = 10^{-6} . Section 9 ($> 10 \mu\text{m}$) data is not available

Size Bin	NH ₄ ⁺		SO ₄ ²⁻		NO ₃ ⁻		Cl ⁻		H ₂ O	
1	-1.1483%	-0.4633%	-0.0488%	-0.0488%	-1.4212%	-0.5717%	0.0000%	0.0000%	N/A	N/A
2	0.6984%	0.0803%	0.0062%	0.0000%	1.1393%	0.1471%	0.0308%	0.0308%	N/A	N/A
3	0.3754%	0.1026%	-0.0018%	-0.0018%	0.6015%	0.1504%	0.0024%	0.0024%	N/A	N/A
4	0.0452%	0.0685%	0.0000%	0.0000%	0.1113%	0.1660%	0.0051%	0.0051%	N/A	N/A
5	0.0499%	0.0856%	0.0035%	0.0035%	0.1779%	0.3246%	-0.0071%	-0.0071%	N/A	N/A
6	0.0376%	0.0602%	-0.0113%	-0.0113%	0.0902%	0.1353%	-0.0146%	-0.0146%	0.0394%	0.0526%
7	0.0072%	0.0145%	0.0071%	0.0071%	0.0092%	0.0163%	-0.0012%	-0.0012%	0.0114%	0.0152%
8	0.0042%	0.0014%	0.0053%	0.0053%	0.0197%	0.0158%	0.0472%	0.1003%	-0.0163%	-0.0245%
9	N/A	N/A	N/A	N/A	N/A	N/A	N/A	N/A	N/A	N/A
Gas	NH ₃ (g)		H ₂ SO ₄ (g)		HNO ₃ (g)		HCl(g)			
	-0.0086%	-0.0037%	-1.2108%	1.5382%	-0.0871%	-0.0378%	-0.0481%	-0.1449%		

Table 7

Normalized errors for Los Angeles evaporation case. ATS: $\varepsilon = 0.1$ (left) and 0.01 (right); LSODE: RTOL = 10^{-5} , ATOL = 10^{-8} . Section 9 ($> 10 \mu\text{m}$) data is not available

Size bin	NH ₄ ⁺		SO ₄ ²⁻		NO ₃ ⁻		Cl ⁻		H ₂ O	
1	0.0163%	-0.0012%	0.0037%	0.0037%	-0.0021%	-0.0349%	3.2380%	-0.2262%	N/A	N/A
2	-0.5511%	-0.4076%	-0.0012%	-0.0012%	0.3916%	0.2845%	0.2554%	0.1985%	N/A	N/A
3	0.0018%	0.0018%	0.0008%	-0.0011%	0.0201%	0.0099%	0.0295%	0.0192%	N/A	N/A
4	0.0016%	0.0016%	0.0018%	0.0018%	0.0202%	0.0099%	0.0318%	0.0240%	N/A	N/A
5	-0.0301%	-0.0202%	-0.0001%	-0.0001%	-0.1042%	-0.0714%	0.0127%	0.0127%	N/A	N/A
6	-0.0163%	0.0001%	-0.0001%	-0.0001%	-0.0212%	0.0021%	-0.3243%	-0.1799%	-0.0146%	0.0012%
7	-0.0197%	-0.0124%	0.0001%	0.0001%	-0.0058%	-0.0058%	-0.0987%	-0.0681%	-0.0178%	-0.0121%
8	-0.0049%	-0.0038%	0.0005%	0.0005%	-0.0036%	-0.0036%	-0.0076%	-0.0050%	-0.0052%	-0.0052%
9	N/A	N/A	N/A	N/A	N/A	N/A	N/A	N/A	N/A	N/A
Gas	NH ₃ (g)		H ₂ SO ₄ (g)		HNO ₃ (g)		HCl(g)			
	0.0055%	0.0036%	-0.3885%	-2.6627%	0.0130%	0.0052%	0.0206%	0.0163%		

Table 8

Normalized errors for Riverside condensation case. ATS: $\varepsilon = 0.1$ (left) and 0.01 (right); LSOE: RTOL = 10^{-7} , ATOL = 10^{-6} . Section 9 ($> 10 \mu\text{m}$) data is not available

Size bin	NH_4^+		SO_4^{2-}		NO_3^-		Cl^-		H_2O	
1	0.1639%	0.8689%	-0.0226%	-0.0181%	0.2712%	1.3273%	-4.8980%	0.4000%	N/A	N/A
2	0.3188%	-0.2601%	-0.0091%	-0.0091%	0.4588%	-0.4215%	0.2517%	-0.2117%	N/A	N/A
3	0.2432%	-0.1179%	0.0099%	0.0099%	0.3986%	-0.1651%	0.2418%	-0.0484%	N/A	N/A
4	-0.1084%	-0.0917%	-0.0034%	-0.0034%	-0.1575%	-0.1248%	-0.0609%	-0.0376%	N/A	N/A
5	-0.0817%	-0.0891%	0.0073%	0.0073%	-0.0317%	-0.0268%	0.0316%	0.0299%	N/A	N/A
6	-0.0227%	-0.0209%	0.0000%	0.0000%	0.0277%	0.0333%	-0.1468%	-0.0695%	0.0757%	0.0879%
7	-0.0100%	-0.0050%	0.0000%	0.0000%	0.0027%	0.0123%	-0.2259%	-0.1927%	-0.0117%	0.0039%
8	-0.0119%	-0.0119%	0.0061%	0.0061%	0.0000%	0.0000%	-0.0014%	0.0084%	-0.0036%	0.0018%
9	N/A	N/A	N/A	N/A	N/A	N/A	N/A	N/A	N/A	N/A
Gas	$\text{NH}_3(\text{g})$		$\text{H}_2\text{SO}_4(\text{g})$		$\text{HNO}_3(\text{g})$		$\text{HCl}(\text{g})$			
	0.0017%	0.0033%	N/A	N/A	-0.0038%	-0.0052%	0.0652%	0.0182%		

Table 9

Normalized errors for Riverside evaporation case. ATS: $\varepsilon = 0.1$ (left) and 0.01 (right); LSOE: RTOL = 10^{-7} , ATOL = 10^{-8} . Section 9 ($> 10 \mu\text{m}$) data is not available

Size bin	NH_4^+		SO_4^{2+}		NO_3^-		Cl^-		H_2O	
1	0.5874%	0.3196%	0.0009%	0.0009%	2.9704%	1.6047%	-0.0483%	-0.0539%	N/A	N/A
2	0.2929%	0.1664%	0.0026%	0.0026%	2.3478%	1.3466%	-0.1279%	-0.1234%	N/A	N/A
3	-1.0616%	-0.1479%	0.0025%	0.0025%	-2.8484%	-0.3531%	0.0214%	0.0446%	N/A	N/A
4	-0.2357%	-0.2826%	0.0036%	0.0036%	-0.3208%	-0.3832%	0.0961%	0.1242%	N/A	N/A
5	-0.0249%	-0.0918%	0.0019%	0.0019%	0.0591%	-0.0260%	0.2970%	0.2937%	0.0000%	0.0000%
6	0.0042%	-0.0286%	0.0034%	0.0034%	0.0005%	-0.0243%	-0.0167%	0.0193%	-0.0008%	-0.0142%
7	0.0096%	-0.0011%	0.0044%	0.0044%	0.0073%	0.0031%	0.0008%	0.0259%	0.0051%	0.0105%
8	0.0018%	-0.0008%	0.0006%	0.0006%	0.0036%	-0.0033%	0.0006%	0.0006%	0.0010%	-0.0011%
9	N/A	N/A	N/A	N/A	N/A	N/A	N/A	N/A	N/A	N/A
Gas	$\text{NH}_3(\text{g})$		$\text{H}_2\text{SO}_4(\text{g})$		$\text{HNO}_3(\text{g})$		$\text{HCl}(\text{g})$			
	0.0345%	0.0283%	N/A	N/A	0.1259%	0.0867%	N/A	N/A		

Table 10

Summary of RMS, CPU times and SDA's (integration time = 12 min)

Test cases		$\varepsilon = 0.1$		$\varepsilon = 0.01$	
		RMSE	CPU time (s)	RMSE	CPU time (s)
Tampa	Cond.	4.7×10^{-3}	0.23	8.6×10^{-4}	0.47
	Evap.	1.7×10^{-2}	0.04	1.3×10^{-3}	0.14
Bakersfield	Cond.	1.0×10^{-2}	0.0024	1.3×10^{-3}	0.013
	Evap.	1.2×10^{-2}	0.0024	5.8×10^{-4}	0.019
Los Angeles	Cond.	4.3×10^{-3}	0.03	2.9×10^{-3}	0.14
	Evap.	5.4×10^{-3}	0.05	1.1×10^{-3}	0.18
Riverside	Cond.	8.0×10^{-3}	0.05	2.9×10^{-3}	0.18
	Evap.	8.0×10^{-3}	0.04	3.6×10^{-3}	0.12
SDA		2.1		2.7	

in urban environments. SDA is around 2.0 for $\varepsilon = 0.1$ and 3.0 for $\varepsilon = 0.01$. To give a comprehensive picture of ATS's speed and accuracy, we plot its

RMSE as a function of CPU times along with Gear for the different test cases in Fig. 3. The various RMSE values for LSOE, LSOE's and VODE

are from different combinations of ATOL and RTOL values. As shown in Fig. 3, ATS generally resides in the left end of the graphs, which indicate that ATS is faster than the other solvers for comparable RMSE values. ATS's computational advantage is most obvious for acidic Tampa cases (Figs. 3a and b), where ATS is 10–100 times faster than the other solvers with equivalent accuracy. For acid neutral cases in Bakersfield, Los Angeles and Riverside, ATS with $\epsilon = 0.1$ exhibits similar 10–100 times overall improvement over all other solvers. In these cases, careful tuning of the LSODES solver's tolerance parameters leads to similar or sometimes slightly better balance between speed and accuracy,

such as shown in Fig. 3d and g, than ATS with $\epsilon = 0.01$. This suggests that composition-dependent tolerance controls could make LSODES desirable for aerosol dynamics simulations. With a single parameter, ϵ , for error control, ATS is more robust than LSODES when implemented in a large domain with a wide range of compositions. It is worth noting that the stiffness in the ODE systems in acid neutral cases have been reduced by coupled transport schemes discussed in Section 3.1.

Besides the realistic cases mentioned above, a hypothetical scenario is also studied to test the robustness of ATS in extreme conditions. In this scenario, we chose particulate phase concentrations,

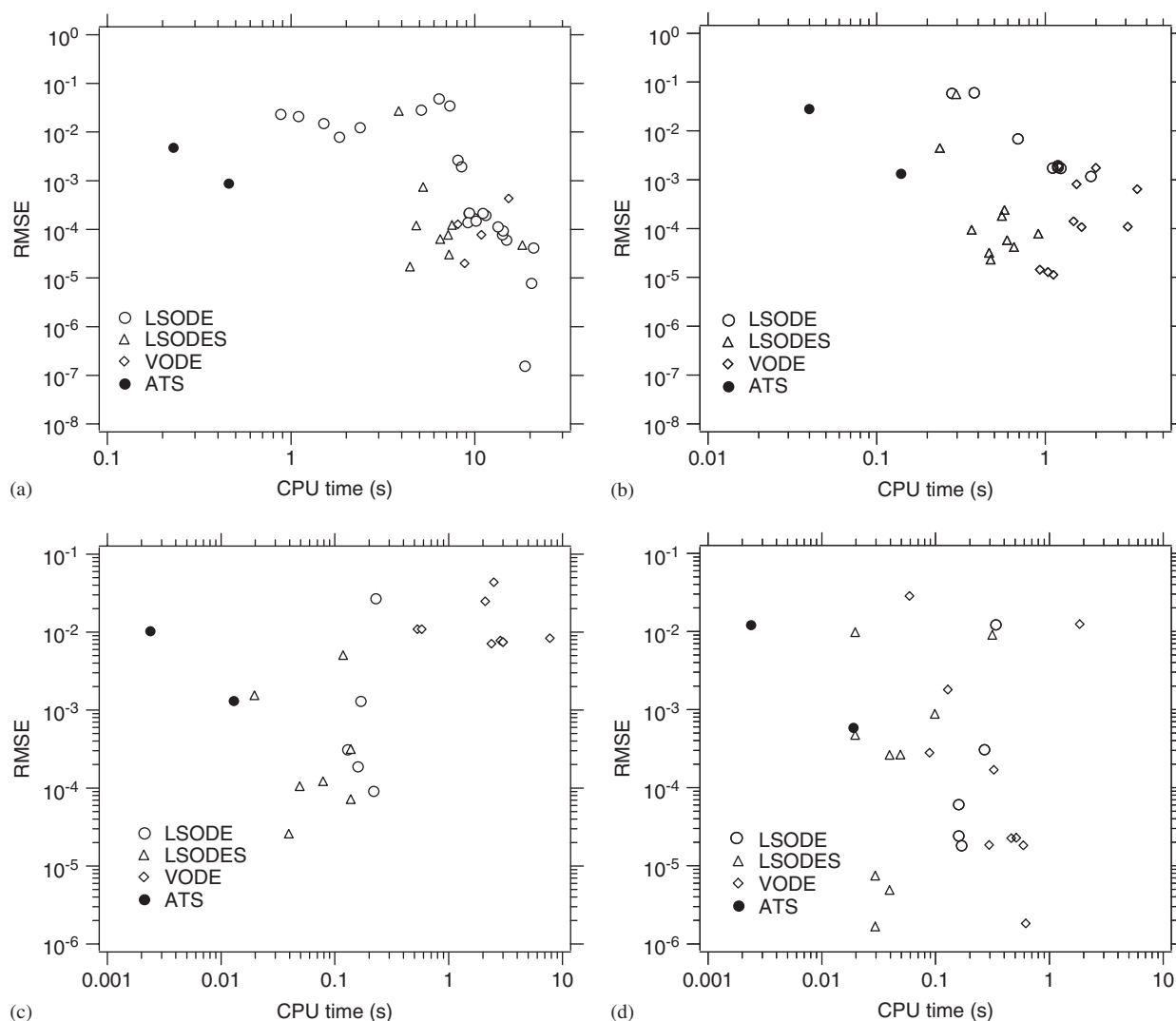


Fig. 3. Comparisons of RMSE and CPU times between Gear and ATS for the eight testing cases: (a) Tampa, condensation; (b) Tampa, evaporation; (c) Bakersfield, condensation; (d) Bakersfield, evaporation; (e) Los Angeles, condensation, (f) Los Angeles, evaporation, (g) Riverside, condensation and (h) Riverside, evaporation.

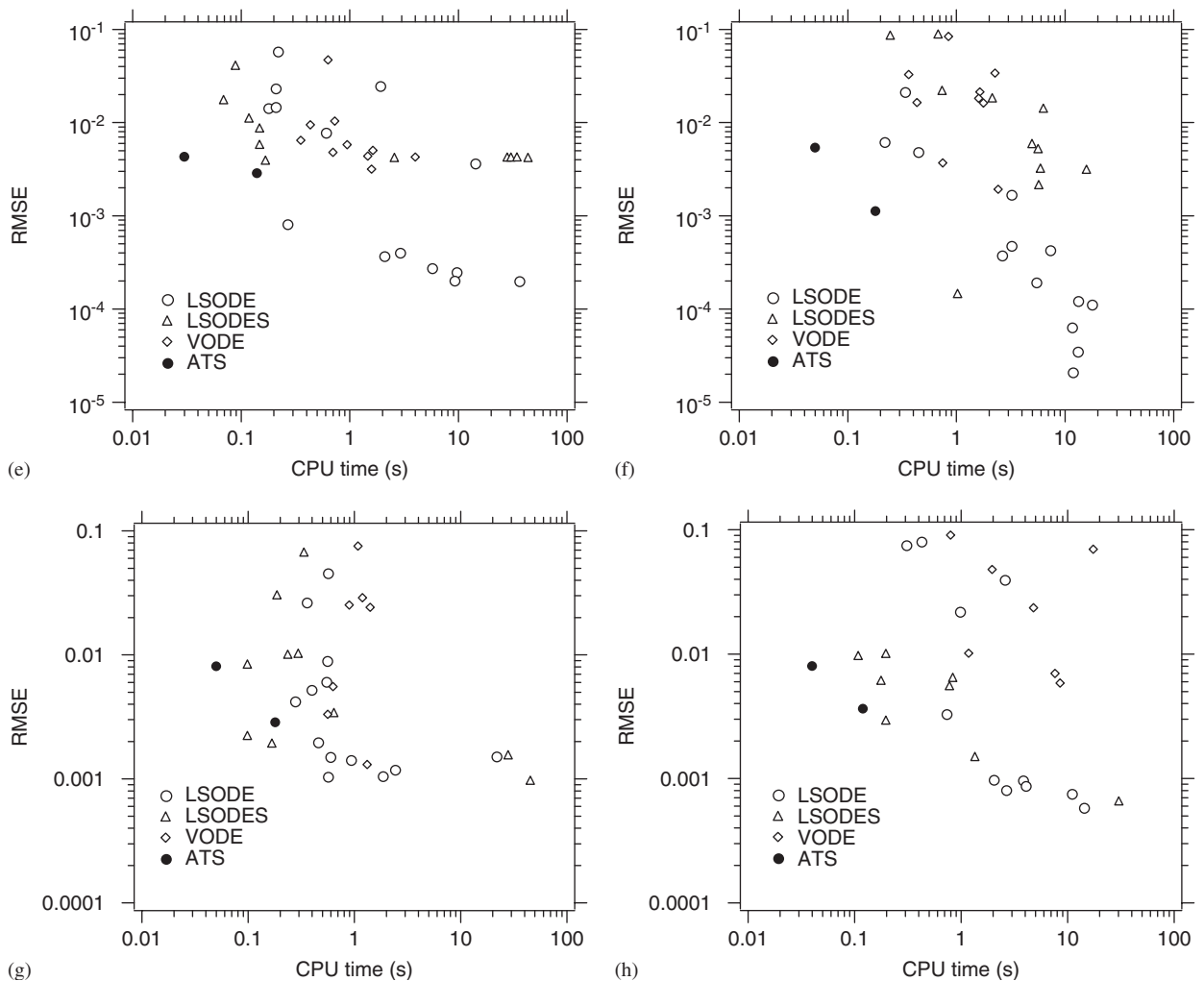


Fig. 3. (Continued)

a generally acidic composition, from Tampa condensation case, but elevated the concentration of the gas phase ammonia to around $10 \mu\text{g m}^{-3}$ higher than its typical values, leading to much faster transition from acidic to neutral composition than what typically occurs. Numerically, this hypothetical case represents a much stiffer ODE system. Fig. 4 presents the time evolution of RMSE for this hypothetical case (Fig. 4a) compared to that of realistic Tampa condensation case (Fig. 4b). In the hypothetical case, the RMSEs reach their peaks after around 1 second of integration as particulate composition approaches acid neutrality and then dampen as composition remains neutral while different size section quickly adjust to equilibrium with the gas phase. The maximum RMSE from 0.01

to 12 mins integration time is 3.0×10^{-2} for ATS with $\varepsilon = 0.1$ and 7.3×10^{-3} for ATS with $\varepsilon = 0.01$. Since the final equilibrium states are generally less dependent on numerical methods, the RMSE's at 12 min integration time, when equilibrium has been achieved, are much smaller ($\sim 10^{-4}$). In contrast, the RMSE's for the realistic Tampa condensation case do not exhibit strong time dependence (Fig. 4b). The maximum and minimum RMSEs for ATS with $\varepsilon = 0.1$ are 5.0×10^{-3} and 1.9×10^{-3} , and the maximum and minimum RMSEs for ATS with $\varepsilon = 0.01$ are 1.6×10^{-3} and 4.0×10^{-4} . In summary, ATS is able to capture the compositional time evolution for this hypothetical case but its accuracy, especially with $\varepsilon = 0.1$, deteriorates as the system becomes very stiff.

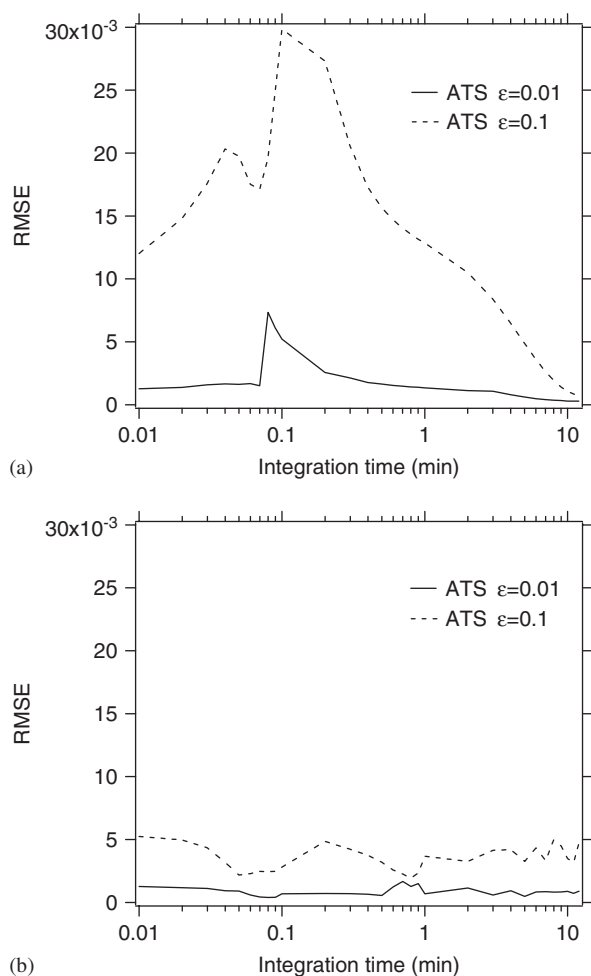


Fig. 4. Time evolution of RMSE for (a) a highly stiff hypothetical case and (b) realistic Tampa condensation case.

4. Conclusion

We developed an asynchronous time-stepping (ATS) integrator for atmospheric applications. ATS traces its origin from the mixed time integration methods, also known as multiple time-step method (MTS), which have been successfully implemented to reduce the stiffness of problems in molecular dynamics and solid mechanics. ATS is able to achieve improved computational efficiency by reducing the numbers of integrations for slow variables and avoiding Jacobian matrix inversion. We adopt several techniques including advanced time management and dynamic ordering to increase the accuracy while maintain this computational efficiency.

Aerosol dynamics simulation requires computationally intensive aerosol thermodynamics calcula-

tions, which do not possess a mathematically straightforward form in contrast to gas chemistry simulations. Particulate compositions and the wide range of particle sizes lead to stiffness in the ODE system. Thus, we optimize ATS for solving stiff ordinary differential equations in aerosol dynamics. Based on the characteristics of the aerosol dynamics system, we group the ODE's representing particulate species by particle size section, and an explicit Euler integration method is employed with a predictor-corrector scheme to maintain its stability. The comparisons between ATS and other ODE solvers, i.e., LSODE, LSODES and VODE, in aerosol dynamics simulation shows that ATS is able to achieve a significant digit average (SDA) value of 1.9–3.0. For acidic cases, ATS's speed is around 10–100 times faster than the other solvers with equivalent accuracy. For acid neutral cases that have reduced stiffness, ATS with $\epsilon = 0.1$ achieved 10–100 times speed improvement while LSODES can match the overall performance of ATS with $\epsilon = 0.01$ only with carefully chosen relative and absolute tolerances. With a single parameter ϵ for error control, ATS is robust and suitable for simulations in a large geographical domain with distinctly different aerosol compositions.

Acknowledgement

This work was supported by US Environmental Protection Agency (USEPA) via a UCAR Fellowship and the California Air Resources Board. The authors want to thank Dr. Robin Dennis at USEPA Atmospheric Modeling Division and the staff in UCAR Visiting Scientist Program for their help.

Reference

- Allen, J.O., Hughes, L.S., Salmon, L.G., Mayo, P.R., Johnson, R.J., Cass, G.R., 2000. Characterization and Evolution of Primary and Secondary Aerosols During PM_{2.5} and PM₁₀ Episodes in the South Coast Air Basin. Coordinating Research Council Technical Report A 22.
- Belytschko, T., Mullen, R., 1976. Mesh partitions of explicit-implicit time integrators. In: Bathe, K.J., Oden, J.T., Wunderlich, W. (Eds.), *Formulations and Computational Algorithms in Finite Element Analysis*. MIT Press, Cambridge, MA, pp. 673–690.
- Belytschko, T., Lu, Y.Y., 1993. Explicit multi-time step integration for 1st and 2nd-order finite-element semidiscretizations. *Computer Methods in Applied Mechanics and Engineering* 108 (3–4), 353–383.

- Brown, P.N., Byrne, G.D., Hindmarsh, A.C., 1989. VODE—A variable-coefficient ODE solver. *SIAM Journal on Scientific and Statistical Computing* 10 (5), 1038–1051.
- Campbell, S.W., Evans, M.C., Poor, N.D., 2002. Predictions of size-resolved aerosol concentrations of ammonium, chloride and nitrate at a bayside site using EQUISOLV II. *Atmospheric Environment* 36 (27), 4299–4307.
- Capaldo, K.P., Christodoulos, P., Pandis, S.N., 2000. A computationally efficient hybrid approach for dynamic gas/aerosol transfer in air quality models. *Atmospheric Environment* 34, 3617–3627.
- Eisenstat, S.C., Gursky, M.C., Schultz, M.H., Sherman, A.H., 1977. Yale sparse matrix package: II. The nonsymmetric codes. Research Report No. 114, Dept. of Computer Sciences, Yale University.
- Eisenstat, S.C., Gursky, M.C., Schultz, M.H., Sherman, A.H., 1982. Yale sparse-matrix package. I. The symmetric codes. *International Journal for Numerical Methods in Engineering* 18 (8), 1145–1151.
- Gear, C.W., 1971. The automatic integration of ordinary differential equations. *Communications of the ACM* 14 (3), 176–179.
- Herner, J.D., Aw, J., Gao, O., Chang, D.P., Kleeman, M.J., 2005. Size and composition distribution of airborne particulate matter in northern California: I-particulate mass, carbon, and water-soluble ions. *Journal of the Air & Waste Management Association* 55 (1), 30–51.
- Hertel, O., Berkowicz, R., Christensen, J., Hov, O., 1993. Test of two numerical schemes for use in atmospheric transport-chemistry models. *Atmospheric Environment* 27A (16), 2591–2611.
- Hesstvedt, E., Hov, O., Isaksen, I.S.A., 1978. Quasi-steady state approximation in air pollution modelling: comparison of two numerical schemes for oxidant prediction. *International Journal of Chemical Kinetics* 10 (9), 971–994.
- Hindmarsh, Alan, C., 1983. ODEPACK. In: Stepleman, R.S., et al. (Eds.), *A Systematized Collection of ODE Solvers*, in *Scientific Computing*. North-Holland, Amsterdam, pp. 55–64.
- Lambert, J.D., 1980. Stiffness. In: Gladwell, I., Sayers, D.K. (Eds.), *Computational Techniques for Ordinary Differential Equations*. Academic press, New York, pp. 19–46.
- Mathur, R., Young, J.O., Schere, K.L., Gipson, G.L., 1998. A comparison of numerical techniques for solution of atmospheric kinetic equations. *Atmospheric Environment* 32 (9), 1535–1553.
- Neal, M.O., Belytschko, T., 1989. Explicit explicit subcycling with non-integer time step ratios for structural dynamic-systems. *Computers & Structures* 31 (6), 871–880.
- Nolte, C., Dennis, R.L., Bhave, P.V., Zhang, K.M., Wexler, A.S., 2006. Application of the CMAQ-UCD aerosol model to a coastal urban site. in preparation.
- Oran, Elaine, S., Jay, P., Boris, 1987. *Numerical simulation of reactive flow*. Elsevier, New York 1987.
- Pilinis, C., Capaldo, K.P., Nenes, A., Pandis, S.N., 2000. MADM—A new multicomponent aerosol dynamics model. *Aerosol Science and Technology* 32 (5), 482–502.
- Smolinski, P., Wu, Y.-S., 1998. An implicit multi-time step integration method for structural dynamics problems. *Computational Mechanics* 22, 337–343.
- Streett, W.B., Tildesley, D.J., Saville, G., 1978. Multiple time-step methods in molecular dynamics. *Molecular Physics* 35 (3), 639–648.
- Sun, Q., Wexler, A.S., 1998. Modeling urban and regional aerosols—Condensation and evaporation near acid neutrality. *Atmospheric Environment* 32 (20), 3527–3531.
- Swindoll, R.D., Haile, J.M., 1984. A multiple time-step method for molecular-dynamics simulations of fluids of chain molecules. *Journal of Computational Physics* 53 (2), 289–298.
- Teleman, O., Jönsson, B., 1986. Vectorizing a general-purpose molecular-dynamics simulation program. *Journal of Computational Chemistry* 7 (1), 58–66.
- Tuckerman, M.E., Martyna, G.J., Berne, B.J., 1990. Molecular-dynamics algorithm for condensed systems with multiple time scales. *Journal of Chemical Physics* 93 (2), 1287–1291.
- Verwer, J.G., Blom, M., van Loon, Spee, E.J., 1996. A comparison of stiff ODE solvers for atmospheric chemistry problem. *Atmospheric Environment* 30 (1), 49–58.
- Wexler, A.S., Seinfeld, J.H., 1990. The distribution of ammonium salts among a size and composition dispersed aerosol. *Atmospheric Environment* 24A (5), 1231–1246.
- Wu, Y.S., Smolinski, P., 2000. A multi-time step integration algorithm for structural dynamics based on the modified trapezoidal rule. *Computer Methods in Applied Mechanics and Engineering* 187, 641–660.
- Young, T.R., Boris, J.P., 1977. A numerical technique for solving stiff ordinary differential equations associated with the chemical kinetics of reactive-flow problems. *The Journal of Physical Chemistry* 81 (25), 2424–2427.
- Zhang, K.M., Wexler, A.S., 2004. Evolution of particle number distribution near roadways—Part I: analysis of aerosol dynamics and its implications for engine emission measurement. *Atmospheric Environment* 38 (38), 6643–6653.
- Zhang, K.M., Wexler, A.S., 2006. Modeling urban and regional aerosols—Development of the UCD aerosol module and implementation in CMAQ-UCD model, in preparation.

Further reading

- Brown, P.N., Hindmarsh, A.C., 1989. Reduced storage matrix-methods in stiff ODE systems. *Applied Mathematics and Computation* 31, 40–91.
- Koo, B., Gaydos, T.M., Pandis, S.N., 2003. Evaluation of the equilibrium, dynamic, and hybrid aerosol modeling approaches. *Aerosol Science and Technology* (37), 53–64.